Opto-Electronic Advances

CN 51-1781/TN ISSN (Print) 2096-4579 ISSN (Online) 2097-3993

Ultra-high-capacity full-vectorial meta-holography

Dengji He, Yuanjian Wan, Yajuan Dong, Yu Wang, Xiaotong Zhu, Tao Wang, Jinwei Zeng* and Jian Wang*

Citation: He DJ, Wan YJ, Dong YJ, Wang Y, Zhu XT, Wang T, Zeng JW, Wang J. Ultra-high-capacity full-vectorial meta-holography. *Opto-Electron Adv* **9**, 250281 (2026).

https://doi.org/10.29026/oea.2026.250281

Received: 24 October 2025; Accepted: 26 January 2026; Published online: 24 March 2026

Related articles

Opto-Electronic Advances

Article

2026, Vol. , No.

Open Access

Ultra-high-capacity full-vectorial meta-holography

Dengji He[1,2,3†], Yuanjian Wan[1,2,3†], Yajuan Dong[1,2,3], Yu Wang[1,2,3], Xiaotong Zhu[1,2,3], Tao Wang[1,2,3], Jinwei Zeng[1,2,3*] and Jian Wang[1,2,3*]

Abstract: Vectorial metasurface holography is a powerful technique that relies on full-dimensional modulation of optical fields to realize its full potential, laying the foundation for encoding vast amounts of optical information and enhancing optical encryption. However, current methods for achieving such modulation remain challenging, as they typically require tuning multiple structural parameters or employing multilayer metasurfaces to provide sufficient degrees of control. Here, we propose a broadband full-vectorial meta-holography (BFVM) strategy based on a purely dielectric geometric-phase metasurface, which achieves complete control over the amplitude, phase, inhomogeneous polarization, and position of light solely by varying the rotation angles of the meta-units. This approach not only enables the generation of full-vectorial holographic images with complete Stokes polarization distributions, but also supports the creation of up to 50 distinct, ultra-high-capacity vectorial holograms, each encoding a designed polarization structure with spatial variation. These structured polarization states can serve as a previously overlooked degree of freedom for enhancing holographic storage. This advancement expands the frontier of vectorial holography, paving the way for next-generation full-vectorial beam shaping, full-color holographic displays, and immersive AR/VR technologies.

Keywords: metasurface; full-dimensional modulation; vectorial holography

DOI: 10.29026/oea.2026.250281 | CSTR: 32247.14.oea.2026.250281

Citation: He DJ, Wan YJ, Dong YJ et al. Ultra-high-capacity full-vectorial meta-holography. *Opto-Electron Adv*, 250281 (2026).

1 Introduction

Vectorial holography is an advanced optical technique that enables precise manipulation of amplitude, phase, and inhomogeneous polarization in holographic imaging[1–3]. Unlike conventional scalar holography, which primarily modulates intensity and phase, vectorial holography fully exploits light's degrees of freedom, allowing for the generation of structured light fields with arbitrarily tailored polarization distributions. It lays a foundational framework for next-generation optical systems, with transformative implications for data storage, secure optical encryption, and advanced display technologies[4–9]. Among various implementation strategies, metasurfaces[10–14]—comprising subwavelength engineered structural units —have emerged as an exceptionally powerful platform for precise wavefront manipulation[15–24]. Over the past decade, they have been successfully applied in a wide range of applications, including orbital angular momentum (OAM) detection[25], spectropolarimetric detection[26], broadband 3D holography[9], and structured light generation[27]. Their unparalleled capability to tailor electromagnetic wave properties with subwavelength precision has also established them as a pivotal enabler of compact, efficient, and versatile vectorial holography, commonly known as vectorial metasurface holography[28–36].

Recent progress in metasurface engineering has enabled the creation of vectorial holograms with tailored optical responses, paving the way for applications in high-security optical encryption, multichannel information processing and high-capacity optical information storage[37–39]. For instance, Yu et al. employed geometric-phase metasurfaces to realize multi-channel vectorial holography by harnessing spin-orbit-locked vortex beams[40]. Furthermore, Zhao et al. integrated propagation phase into geometric-phase designs to enable vectorial holographic display across multiple information channels[41]. Moreover, Kim et al. developed bi-layer

Received: 24 October 2025

Accepted: 26 January 2026

Published online: 24 March 2026

[1]Wuhan National Laboratory for Optoelectronics and School of Optical and Electronic Information, Huazhong University of Science and Technology, Wuhan, 430074, China; [2]Hubei Optical Fundamental Research Center, Wuhan 430074, China; [3]Optics Valley Laboratory, Wuhan 430074, China.

†These authors contributed equally to this work.

*Correspondence: JW Zeng, E-mail: zengjinwei@hust.edu.cn; J Wang, E-mail: jwang@hust.edu.cn

metasurfaces to achieve bidirectional vectorial holography and demonstrated its effectiveness in secure optical encryption[42]. Despite these advancements, achieving broadband full-vectorial holography using a single-layer metasurface based purely on geometric phase remains a significant challenge, as true full-vectorial holography requires the metasurface to independently and flexibly control the amplitude, phase, and arbitrary polarization states of the optical field—capabilities that are difficult to achieve solely through the rotation of units.

In this study, we propose a broadband full-vectorial meta-holography (BFVM) strategy based on a purely dielectric geometric-phase metasurface capable of full-dimensional modulation of the optical field—including amplitude, phase, polarization, and spatial position. Compared with conventional vectorial holography based on bulk optical components, and metasurface-based implementations that rely on multilayer architectures or multiple structural parameters, our approach achieves simultaneous and independent control of all four optical degrees of freedom solely through rotation-angle encoding on a single-layer metasurface. This design offers significant advantages in terms of structural simplicity, device compactness, and broadband functionality. In this work, the term "full vectorial" specifically refers to the capability of producing arbitrary output polarization states (including linear, circular, and elliptical polarization) under fixed input polarization conditions. We validate the performance of this approach both theoretically and experimentally by demonstrating three distinct vectorial holograms, each featuring spatially tailored polarization characteristics, where the upper and lower regions are encoded with customized linear or circular polarization states. Collectively, these holograms span the full Stokes polarization space, confirming the system's capability for complete vectorial field control. To further extend the capacity of vectorial holography, we implement a full-dimensional modulation metasurface capable of producing up to 50 distinct vectorial holographic patterns, each featuring spatially variant polarization distributions (e.g., radial or azimuthal polarization distributions). Notably, our approach unveils a previously overlooked degree of freedom in holographic storage, allowing independent control of vectorial polarization-encoded information while preserving the reconstructed intensity distribution. This work substantially enhances the multi-channel information capacity of vectorial optical encryption, improves decryption robustness, and opens promising new directions for secure encryption and high-density optical data storage.

2 Results

2.1 Design principle of full-dimensional metasurface modulation

As illustrated in Fig. 1, we propose a novel full-dimensional modulation metasurface capable of simultaneously, arbitrarily and independently controlling the amplitude, phase, polarization state, and spatial distribution of light, thereby enabling the full access of complete degrees of freedom in wavefront shaping. This metasurface is constructed from meticulously engineered anisotropic meta-atoms, offering precise geometric phase manipulation and polarization-dependent responses, with excellent performance maintained across the visible spectrum. The system demonstrates ultra-high-capacity vectorial meta-holographic channels, each uniquely associated with a specific spatially variant vectorial polarization state, such as radial or azimuthal polarization distributions. Notably, the proposed design can flexibly generate vectorial holograms carrying arbitrarily complex, spatially variant polarization patterns without increasing structural design complexity. Through this multi-dimensional multiplexing strategy, we achieve full-dimensional modulation of optical fields on a single metasurface chip, offering a significant solution for high-density optical data storage and dynamic holographic display applications.

According to the geometric phase modulation mechanism[43–45], precisely oriented anisotropic elements with azimuthal angle θ can perform the conversion $|L\rangle \rightarrow e^{i2\theta}|R\rangle$ and $|R\rangle \rightarrow e^{-i2\theta}|L\rangle$, i.e., such structured media implement spin-selective phase encoding: the the left-handed circularly polarized (LCP) and right-handed circularly polarized (RCP) beams are transformed to opposite spin with a geometric phase (Pancharatnam-Berry phase) of 2θ and -2θ, respectively.

Through geometric phase manipulation, conventional metasurfaces typically achieve only phase modulation of transmitted light. Here we demonstrate a dielectric geometric phase metasurface capable of complete wavefront control via parallel meta-atom design. This full-dimensional modulation platform enables the generation of arbitrary optical fields E_{out} with customized spatial amplitude, phase, polarization and spatial position distributions at the metasurface's near-field transmission plane when illuminated by a linearly polarized (x-polarized) plane wave E_{in}. For mathematical convenience, we represent the incident plane wave and the generated arbitrary light beam in terms of a circular polarization basis, which can be expressed as

$$E_{\text{in}} = \frac{\sqrt{2}}{2}A_0\begin{bmatrix}1\\1\end{bmatrix},$$

$$E_{\text{out}}(x,y) = A(x,y)e^{i\varphi(x,y)}\begin{bmatrix}|E_l(x,y)|\cdot e^{-i\delta_0(x,y)/2}\\|E_r(x,y)|\cdot e^{i\delta_0(x,y)/2}\end{bmatrix}, \quad (1)$$

where A_0 is the amplitude of the incident plane wave, $A(x,y)$, $\varphi(x,y)$, $|E_l(x,y)|$, $|E_r(x,y)|$ and $\delta_0(x,y)$ are the amplitude profile, phase profile, normalized amplitude profile of the LCP component, normalized amplitude profile of the RCP component, and relative phase difference profile between the LCP and RCP components of the produced arbitrary light beam, respectively.

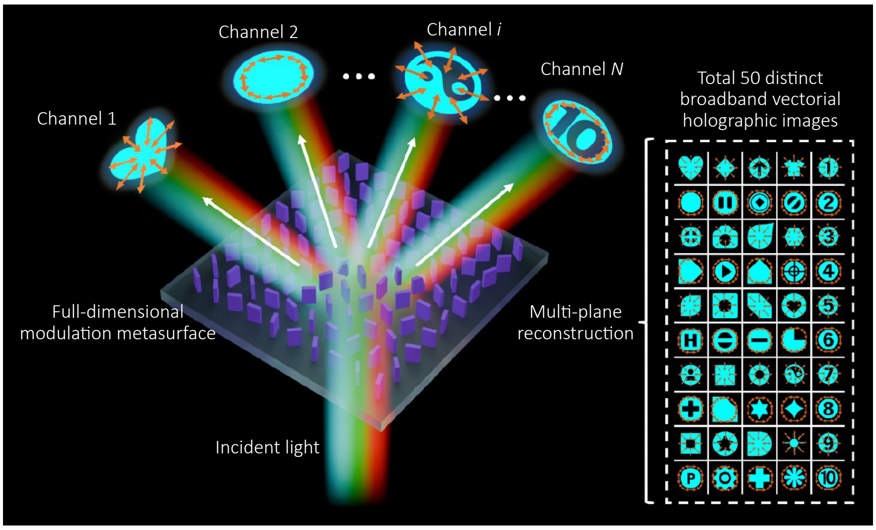

Fig. 1 | Concept of ultra-high-capacity vectorial meta-holography via full-dimensional metasurface modulation. Schematic illustration of a dielectric metasurface with full-dimensional modulation, enabling the generation of ultra-high-capacity vectorial meta-holographic channels. All holographic images feature precisely controllable and complex spatially variant vectorial polarization states, such as radial and azimuthal polarization distributions.

Here, we define a 2×2 supercell, composed of anisotropic unit cells, as the fundamental building block of the metasurface. The material and structural parameters (L = 0.32 μm, W = 0.1 μm, H = 0.55 μm) are presented in Fig. 2(a). Then, we divide the rotating angle of each unit cells ($\theta_1 \sim \theta_4$) into three sub-angles θ_φ, θ_i and θ_s as linear superposition, i.e., $\theta_j = \theta_{j\varphi} + \theta_{ji} + \theta_{js}, j = 1,2,3,4$ (Fig. 2(b)). In addition, the supercell period is denoted as P=0.76 μm. The first sub-angle, θ_φ, modulates the phase profile of the transmitted light by geometric phase mechanism. While the second sub-angle, θ_i, governs its amplitude distribution. Specifically, opposite values of θ_i to adjacent unit cells (e.g., $\theta_{1i} = -\theta_{2i}, \theta_{3i} = -\theta_{4i}$) within each row. As a result, the amplitude of the resulting interference beam for the RCP component can be expressed as: $E^{\mathrm{RCP}}_{\mathrm{interference}} = \mathrm{e}^{\mathrm{i}\varphi_{1i}} + \mathrm{e}^{\mathrm{i}\varphi_{2i}} = \cos(2\theta_{1i})$. Likewise, the amplitude of the interference beam for the LCP component is given by $E^{\mathrm{LCP}}_{\mathrm{interference}} = \mathrm{e}^{\mathrm{i}\varphi_{3i}} + \mathrm{e}^{\mathrm{i}\varphi_{4i}} = \cos(2\theta_{3i})$. Therefore, the amplitude of the target field can be continuously tuned from 0 to 1 by varying the second sub-angle, θ_i. Meanwhile, the third sub-angle, θ_s, operates in conjunction with θ_φ and θ_i to modulate the polarization profile and control the diffraction angle of the transmitted light. Collectively, these three sub-angles enable independent modulation of the transmitted light's spatial amplitude, phase, polarization, and spatial position distributions, with the spatial position determined by the diffraction angle. The relationship between the transmitted light and the rotation angles of the unit cells can be expressed as

$$\begin{aligned}
\theta_1 &= \theta_{1\varphi} + \theta_{1i} + \theta_{1s} = \frac{\varphi(x,y) + \delta_0(x,y)/2 + \arccos[A(x,y)|E_{\mathrm{r}}(x,y)|]}{2} + kr(x,y)\ , \\
\theta_2 &= \theta_{2\varphi} + \theta_{2i} + \theta_{2s} = \frac{\varphi(x,y) + \delta_0(x,y)/2 - \arccos[A(x,y)|E_{\mathrm{r}}(x,y)|]}{2} + kr(x,y)\ , \\
\theta_3 &= \theta_{3\varphi} + \theta_{3i} + \theta_{3s} = -\frac{\varphi(x,y) - \delta_0(x,y)/2 - \arccos[A(x,y)|E_{\mathrm{l}}(x,y)|]}{2} - kr(x,y)\ , \\
\theta_4 &= \theta_{4\varphi} + \theta_{4i} + \theta_{4s} = -\frac{\varphi(x,y) - \delta_0(x,y)/2 + \arccos[A(x,y)|E_{\mathrm{l}}(x,y)|]}{2} - kr(x,y)\ .
\end{aligned} \tag{2}$$

Leveraging the parallel-tasking mechanism, our method enables comprehensive modulation of transmitted light, offering unprecedented control over its amplitude, phase, polarization, and spatial distribution. A rigorous mathematical derivation, along with the final analytical expressions, is provided in the Supplementary Section 1. In addition, the full-dimensional modulation inherently gives rise to a twin optical field alongside the target field. A detailed discussion of this twin field is provided in the Supplementary Section 8. Accordingly, all target holographic patterns presented in this work are obtained by spatially filtering the desired signal through an aperture.

As shown in Fig. 2(c), we numerically simulate the transmission phase spectrum for orthogonally polarized light under LCP illumination to validate the phase modulation capability of the designed element. Due to symmetry, only LCP results are presented. The phase shift exhibits an almost linear relationship with the orientation angle of the element.

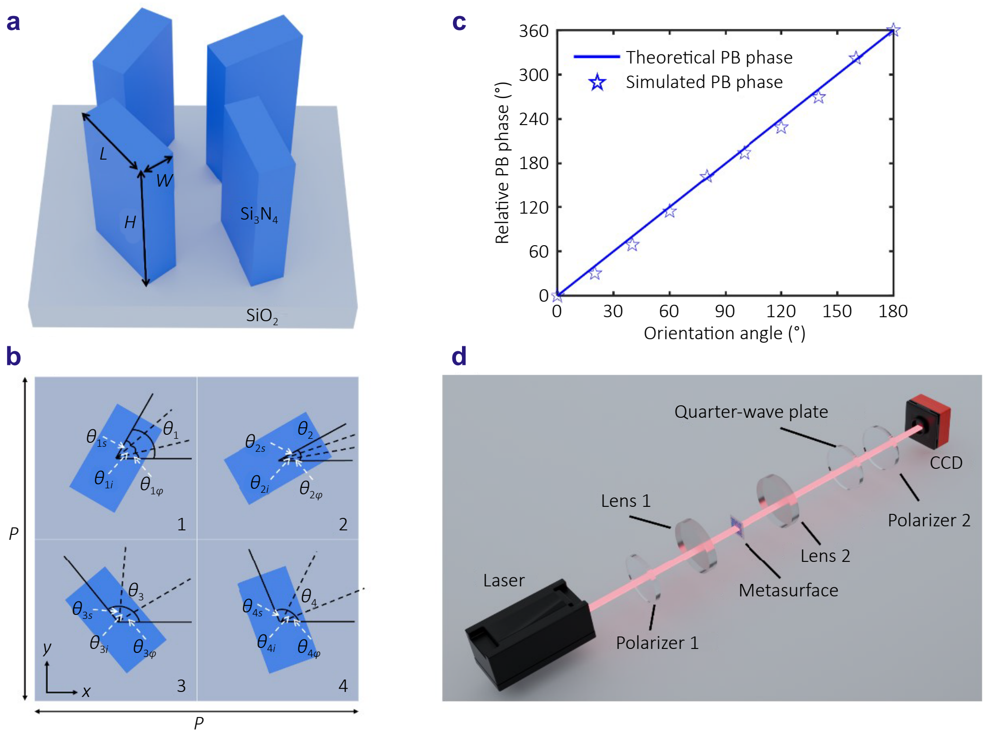

Fig. 2 | Schematic of the designed supercell for full-dimensional modulation metasurface and experimental setup. (a) Side view of the designed supercell of a full-dimensional modulation metasurface. (b) Top view of a supercell of metasurface, where the total orientation angle of each element is decomposed into three sub-angles to facilitate parallel modulation tasks. (c) Relationship between the phase shift and the rotation angle of the dielectric unit. (d) Experimental setup used for capturing vectorial meta-holographic images.

Figure 2(d) illustrates the experimental setup, in which the desired linear polarization (LP) incident light is generated using polarizer 1. The various polarization components of the transmitted field from the metasurface are extracted using polarizer 2 and a quarter-wave plate. The camera captures the holographic patterns after the transmitted light passing through the polarizer. By precisely adjusting the position and polarization angle of the polarizer, the target image can be accurately obtained. Further details of the experimental setup can be found in the Supplementary Section 4.

2.2 Meta-holographic images with spatially varying polarization states

Our full-dimensional modulation approach enables the independent generation of arbitrary amplitude and phase distributions at distinct spatial positions while precisely controlling arbitrary polarization states. This capability advances full-vectorial meta-holography, allowing for the reconstruction of holographic images with spatially variant polarization characteristics. To achieve such a full-vectorial meta-hologram, we employ a superposition of circularly polarized holograms, producing an image where polarization varies across different regions. As an illustrative example, we design a vectorial hologram encoding the letters 'J'、'L' and 'G', with polarization states tailored separately for the upper and lower halves of each letter. Specifically, the upper half of 'J' exhibits x-polarization, while the lower half is y-polarized. For 'L', the upper half is polarized at 45°, whereas the lower half is at 135°. Meanwhile, 'G' features RCP in the upper half and LCP in the lower half, forming a representative full-Stokes polarization distribution. These polarization-encoded patterns are visually represented in Fig. 3(a).

Figure 3(b) presents top-view and side-view scanning electron microscopy (SEM) images of the fabricated sample, highlighting the robustness of the fabrication process and high precision achieved in metasurface manufacturing. More details about processing and manufacturing can be found in the Supplementary Section 6. Figure 3(c) displays both simulated and experimentally captured holographic images generated by the metasurface under horizontally polarized incident light. Our approach enables vectorial holographic imaging across a broad spectral range, as demonstrated by reconstructed images at wavelengths of 447 nm, 518 nm, and 637 nm, respectively.

When no polarizer is placed at the output, the full holographic images of the letters 'J'、 'L' and 'G' are clearly observed. To verify the polarization-encoded features, we place a linear and a circular polarizer at the output side of the metasurface. Under horizontally or vertically aligned polarizers, the lower and upper halves of 'J' disappear,

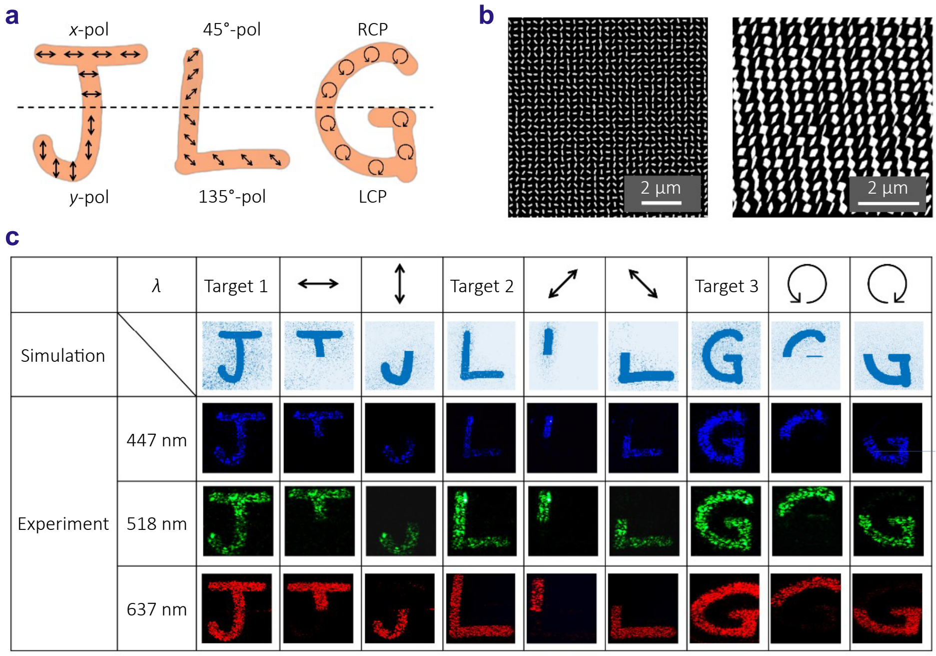

Fig. 3 | Broadband full-vectorial hologram with spatially variant polarization states. (a) Schematic illustration of the designed vectorial hologram, where the upper and lower regions are distinctly encoded with customized linear or circular polarization states under LP incident light. (b) Top-view and side-view SEM images of the fabricated metasurface. (c) Simulated and experimentally captured holographic images at wavelengths of 447 nm, 518 nm, and 637 nm, respectively, obtained by placing different polarizers at the output side of the metasurface.

respectively, confirming their horizontal and vertical polarization states. Similarly, with a 45° or 135° linear polarizer, the corresponding halves of 'L' vanish, consistent with the designed polarization orientations. To further validate the spatially variant circular polarization states, a circular polarizer —comprising a quarter-wave plate and a linear polarizer —is applied at the output. Under this condition, the corresponding halves of 'G' disappear, confirming the presence of RCP and LCP, respectively. These results conclusively demonstrate that the designed metasurface effectively generates holographic images with spatially encoded polarization characteristics.

2.3 Implementation framework for ultra-high-capacity vectorial meta-holograms

To fully explore the data storage potential of the BFVM strategy proposed in this work, we design a series of vectorial meta-holograms featuring uniquely structured and spatially variant vectorial polarization distributions. Considering two orthogonally circularly polarized components of the vectorial hologram carry OAM phases with distinct topological charges, which can be expressed as follows

$$E_{\text{sup}} = E_{\text{image}}(x,y)\cdot \mathrm{e}^{\mathrm{i}\cdot l_1\varphi(x,y)}\begin{bmatrix}1\\ \mathrm{i}\end{bmatrix} + E_{\text{image}}(x,y)\cdot \mathrm{e}^{\mathrm{i}\cdot l_2\varphi(x,y)}\begin{bmatrix}1\\ -\mathrm{i}\end{bmatrix}, \tag{3}$$

where $\begin{bmatrix}1\\ \pm\mathrm{i}\end{bmatrix}$ represents the RCP and LCP states, $E_{\text{image}}(x,y)$ represents the complex amplitude distribution of vectorial holograms, x, y are the coordinate of vectorial holograms, $\varphi(x,y)=\tan^{-1}(x/y)$ is defined as the azimuthal angle, and l is the topological charge.

For two circular polarization components with opposite topological charges, Eq. (3) can be rewritten as

$$\begin{aligned}E_{\text{sup}} &= E_{\text{image}}(x,y)\cdot \mathrm{e}^{\mathrm{i}\cdot l\varphi(x,y)}\begin{bmatrix}1\\ \mathrm{i}\end{bmatrix} + E_{\text{image}}(x,y)\cdot \mathrm{e}^{-\mathrm{i}\cdot l\varphi(x,y)}\begin{bmatrix}1\\ -\mathrm{i}\end{bmatrix}\\ &= 2E_{\text{image}}(x,y)\cdot\begin{bmatrix}\cos(l\varphi(x,y))\\ -\sin(l\varphi(x,y))\end{bmatrix}.\end{aligned} \tag{4}$$

In this case, the superposition of two circularly polarized components generates a vectorial hologram with a radially polarized distribution.

Assuming that there is a phase difference of π between the two circular polarization components, Eq. (4) becomes

$$\begin{aligned}E_{\text{sup}} &= E_{\text{image}}(x,y)\cdot \mathrm{e}^{\mathrm{i}\cdot l\varphi(x,y)}\begin{bmatrix}1\\ \mathrm{i}\end{bmatrix} + E_{\text{image}}(x,y)\cdot \mathrm{e}^{\mathrm{i}\pi}\cdot \mathrm{e}^{-\mathrm{i}\cdot l\varphi(x,y)}\begin{bmatrix}1\\ -i\end{bmatrix}\\ &= 2\mathrm{i}E_{\text{image}}(x,y)\cdot\begin{bmatrix}\sin(l\varphi(x,y))\\ \cos(l\varphi(x,y))\end{bmatrix}.\end{aligned} \tag{5}$$

In this case, the superposition of two circularly polarized components generates a vectorial hologram with an azimuthally polarized distribution.

The physical mechanism of ultra-high-capacity vectorial meta-holography via full-dimensional metasurface modulation is demonstrated in Fig. 4. Here, we design a metasurface that generates 50 distinct vectorial holograms arranged in 10 rows and 5 columns, with odd rows exhibiting radial polarization and even rows azimuthal polarization. Notably, the proposed vectorial holography framework inherently supports arbitrary high-order vectorial polarization states, as demonstrated in the Supplementary Section 17. In this work, we focus on a representative case that resembles the well-known polarization distributions of radial and azimuthal polarization beams (RPB and APB).

For odd rows, we decompose each holographic pattern into a superposition of two orthogonal polarization components (Fig. 4(a)). Specifically, we encode opposite topological charges into the LCP and RCP components of image-n, followed by the addition of a shared random phase R_n to ensure a uniform amplitude distribution across the hologram plane. An inverse fast Fourier transform (IFFT) is then applied to convert the target field from the spatial to the frequency domain, yielding the complex amplitude components for each hologram. To display each vectorial holo-

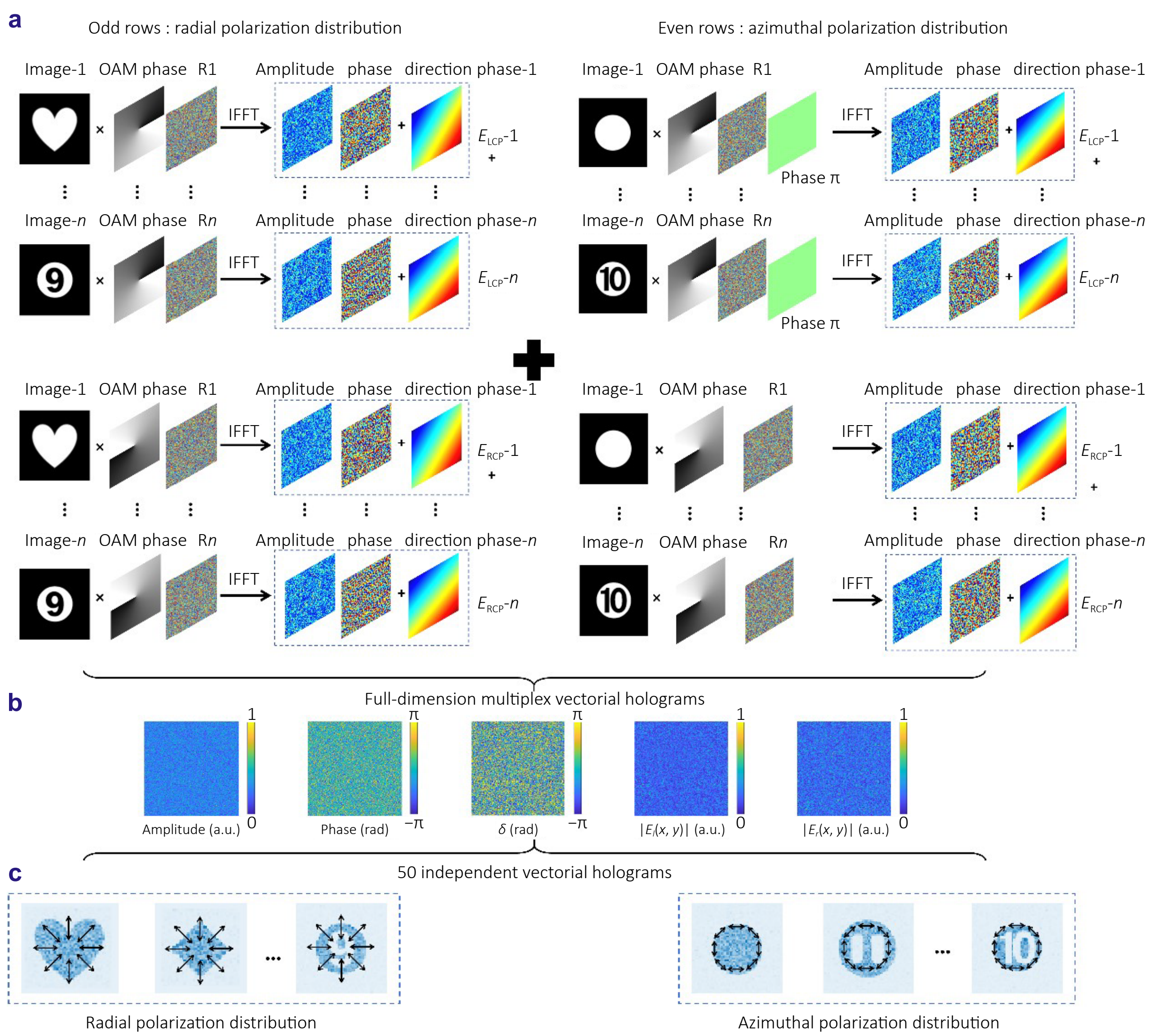

Fig. 4 | The physical mechanism of ultra-high-capacity vectorial meta-holograms technique. (a) The flowchart for implementing ultra-high-capacity BFVM via full-dimensional metasurfaces. For odd rows, each vectorial holographic pattern carrying a radial polarization distribution is synthesized by combining the two orthogonal circularly polarized components with OAM phases of opposite topological charges and a random phase mask. The resulting field is transformed into the spatial domain via IFFT, followed by the incorporation of a directional phase to spatially localize the hologram. For even-numbered rows, an identical procedure is applied, except for the introduction of a π-phase shift to the LCP component before the IFFT. All vectorial holograms are then superimposed at distinct spatial positions, yielding ultra-high-capacity holographic multiplexing. (b) The total electric field distribution required for the metasurface. (c) The designed 50 spatially multiplexing vectorial holographic patterns.

gram at different spatial locations, we introduce a directional phase function that projects the LCP and RCP components to their corresponding positions in space. Superimposing the corresponding LCP and RCP components, we can realize vectorial holographic patterns with radial polarization, uniquely encoded in the odd rows. Each pattern independently carries a radial polarization distribution, representing an advance beyond conventional vectorial metasurface holography methods. For even rows, a constant phase shift of π is introduced to the left circular component before IFFT, while all subsequent steps mirror those of the odd rows.

Following these operations, we obtain the LCP and RCP components required for each vectorial holographic pattern. The metasurface's total electric field distribution is subsequently calculated as the superposition of all channel-modulated optical fields. As shown in Fig. 4(b), we can obtain the resultant metasurface profile, including amplitude profile, phase profile, relative phase difference profile δ between the RCP and LCP components of the multiplexing channel, normalized amplitude profile of RCP component, and normalized amplitude profile of LCP component.

Using Eq. (2) mentioned earlier, we computationally correlate the target field distribution with the geometric-phase-governed rotation angles of the nanostructures, enabling deterministic retrieval of the metasurface element configuration. Ultimately, this results in the realization of 50 spatially multiplexing vectorial meta-holographic patterns, as shown in Fig. 4(c).

2.4 Characterization of ultra-high-capacity vectorial holographic multiplexing

Following the design framework outlined above, we fabricate a metasurface comprising 50 distinct vectorial holograms organized in a 10 × 5 array. The device is 875 μm by 875 μm in size, with representative SEM images of the fabricated metasurface presented in Fig. 5(a). Figure 5(b–d) show

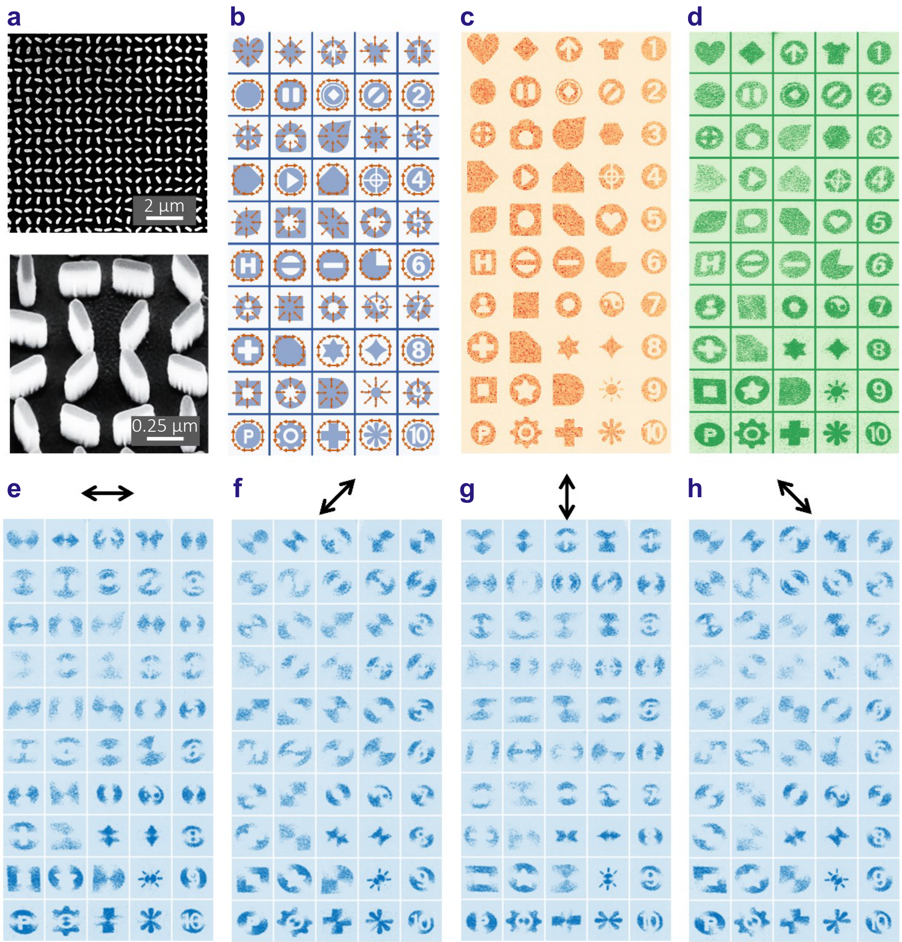

Fig. 5 | Experimental demonstration of ultra-high-capacity vectorial holographic multiplexing. (a) Top-view and side-view SEM images of the fabricated metasurface. (b–d) The target holographic patterns, numerical simulations images, and experimentally reconstructed images obtained without a polarizer. (e–h) The results at 447 nm working wavelength, showing specific dark regions in the reconstructed images, exhibit angular-dependent extinction when the polarizer is rotated through 0°, 45°, 90°, and 135° orientations.

the corresponding target holographic patterns, numerical simulations images, and experimentally reconstructed images obtained without a polarizer, respectively. Throughout the experiments, the incident light is *x*-polarized. Importantly, our design methodology exhibits broadband functionality, and the representative results at 447 nm are shown here. The experimental validation of the device's performance across different wavelengths is provided in the Supplementary Section 9. In addition, we have also provided the complete set of correlation coefficients between the experimental and theoretical results for all 50 reconstructed holographic images, as shown in the Supplementary Section 15. The average correlation coefficient is 0.76, with a standard deviation of 0.07, indicating good device performance and consistency across channels.

To systematically analyze the polarization properties of the generated vectorial meta-holograms, we place a rotating polarizer into the optical path. As shown in Fig. 5(e–h), specific dark regions in the reconstructed images exhibit angular-dependent extinction when the output polarizer is rotated through 0°, 45°, 90°, and 135° orientations. This rotating extinction pattern unambiguously confirms the spatially variant polarization states (radial or azimuthal) encoded within individual holographic elements.

Our full-dimensional metasurface design framework experimentally demonstrates ultra-high-capacity vectorial meta-holography with tailored spatially variant polarization distribution. Furthermore, this approach exhibits inherent compatibility with existing multiplexing strategies to further enhance channel multiplexing capabilities and generate more complex optical fields. It is worth noting that although the experimental results presented in this work may appear visually similar to a conventional vectorial hologram composed of multiple polarization segments, our demonstration of distinct vectorial holographic images is fundamentally different —both in physical encoding principles and functional capabilities. A detailed discussion of this distinction is provided in the Supplementary Section 11.

2.5 Demonstration of additional storage freedom enabled by vectorial polarization in holography

In addition, our approach reveals a previously overlooked degree of freedom in holographic storage, enabling independent control over vectorial polarization-encoded information without altering the reconstructed intensity distribution. This capability establishes vectorial polarization holography as a novel paradigm in information encoding, thereby significantly enhancing the storage capacity of metasurface-based holographic systems, as illustrated in Fig. 6.

Unlike conventional holographic storage, which relies on intensity modulation to encode information, our system exhibits a distinct characteristic: the holographic pattern remains unchanged under varying incident polarization states. This sets it apart from traditional intensity-based holography, where modifications in stored information typically alter the reconstructed image. Figure 6(a, b) show the target and experimental results, which indicate the circular vectorial holographic pattern carries distinct vectorial polarization distributions under different incident polarization

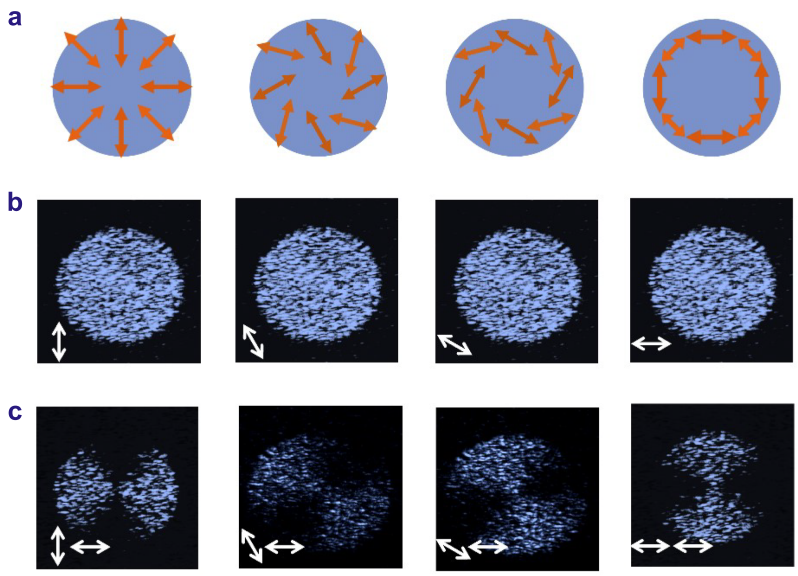

Fig. 6 | Experimental results demonstrating the same circular holographic pattern with varying polarization distributions. (a) The intended polarization distribution within the circular holographic pattern under different incident polarization states. (b) The black arrows in the corners indicate the incident light polarization, with no polarization analyzer applied in the output field. (c) The two black arrows in the corners represent the input (first arrow) and output (second arrow) polarization states, where the varying dark regions correspond to different polarization distributions within the same circular holographic pattern.

states (90°, 120°, 150°, 180°). In our approach, while the light intensity remains unchanged, the spatial vectorial polarization distribution dynamically varies with the incident polarization state.

To intuitively illustrate the vectorial polarization distribution encoded in the holograms, we introduce a fixed linear polarization analyzer in the output field, designed to transmit only the x-polarized component. Under this condition, we systematically rotate the incident polarization state and observe noticeable variations in the holographic image, with certain regions exhibiting dark areas. This phenomenon clearly demonstrates that while the overall holographic intensity distribution remains unchanged, the underlying vectorial polarization distribution is actively modulated by the incident polarization state (as shown in Fig. 6(c)). This suggests that different holographic data channels could be encoded using specific vectorial polarization distributions, thereby expanding the storage capacity of holographic systems.

Therefore, vectorial polarization storage offers additional advantages over scalar polarization encoding in terms of storage capacity. While scalar polarization encoding typically employs a uniform polarization state across the holographic field, vectorial polarization storage exploits spatially variant polarization distributions, which enable multiple distinct information channels to be embedded within the same holographic reconstruction, thereby increasing the effective storage density. Accordingly, vectorial polarization holography represents a complementary and promising approach for high-capacity optical data storage and encryption.

3 Conclusions

In conclusion, we have proposed and experimentally demonstrated an effective full-dimensional optical field manipulation strategy, enabling ultra-high-capacity vectorial meta-holography with virtually unlimited polarization configurations. This approach overcomes the limitations of conventional scalar holography, facilitating the generation of arbitrarily structured light fields with customized polarization states. Future research could focus on extending this approach to non-visible wavelengths, such as infrared and ultraviolet, as well as exploring reconfigurable vectorial holography systems. Additionally, applications in optical encryption offer promising prospects for secure communication and information storage. In addition, to transition towards practical system integration, several challenges remain. These include scaling the metasurface for large-area applications, ensuring robustness under varying environmental conditions, and achieving the required precision in fabrication. Overcoming these challenges will be essential for the practical applications of this technology.

References

1. Wang ZY, Zhou Z, Zhang H et al. Vectorial liquid-crystal holography. *eLight* **4**, 5 (2024).
2. Wan WP, Yang WH, Ye S et al. Tunable full-color vectorial meta-holography. *Adv Opt Mater* **10**, 2201478 (2022).
3. Arbabi E, Kamali SM, Arbabi A et al. Vectorial holograms with a dielectric metasurface: ultimate polarization pattern generation. *ACS Photonics* **6**, 2712–2718 (2019).
4. Zhang X, Ji X, Li X et al. Spatial varying vectorial holography and polarization encryption based on birefringent metasurface. *Adv Funct Mater* **34**, 2404196 (2024).
5. Yang H, He P, Ou K et al. Angular momentum holography via a minimalist metasurface for optical nested encryption. *Light Sci Appl* **12**, 79 (2023).
6. Fan ZX, Qian C, Jia YT et al. Holographic multiplexing metasurface with twisted diffractive neural network. *Nat Commun* **15**, 9416 (2024).
7. Xu K, Liu YC, Fan XH et al. Simultaneous dynamic display of meta-hologram and meta-nanoprinting with high frame rate. *Laser Photon Rev* **19**, 2400815 (2025).
8. Hu YH, Kingsley-Smith JJ, Nikkhou M et al. Structured transverse orbital angular momentum probed by a levitated optomechanical sensor. *Nat Commun* **14**, 2638 (2023).
9. Li X, Chen LW, Li Y et al. Multicolor 3D meta-holography by broadband plasmonic modulation. *Sci Adv* **2**, e1601102 (2016).
10. Yu NF, Capasso F. Flat optics with designer metasurfaces. *Nat Mater* **13**, 139–150 (2014).
11. Yu NF, Genevet P, Kats MA et al. Light propagation with phase discontinuities: generalized laws of reflection and refraction. *Science* **334**, 333–337 (2011).
12. Wang Z, Li TT, Soman A et al. On-chip wavefront shaping with dielectric metasurface. *Nat Commun* **10**, 3547 (2019).
13. Kildishev AV, Boltasseva A, Shalaev VM. Planar photonics with metasurfaces. *Science* **339**, 1232009 (2013).
14. Xiong B, Liu Y, Xu YH et al. Breaking the limitation of polarization multiplexing in optical metasurfaces with engineered noise. *Science* **379**, 294–299 (2023).
15. Chen WT, Zhu AY, Sisler J et al. A broadband achromatic polarization-insensitive metalens consisting of anisotropic nanostructures. *Nat Commun* **10**, 355 (2019).
16. Kwon H, Arbabi E, Kamali SM et al. Single-shot quantitative phase gradient microscopy using a system of multifunctional metasurfaces. *Nat Photonics* **14**, 109–114 (2020).
17. Dorrah AH, Rubin NA, Zaidi A et al. Metasurface optics for on-demand polarization transformations along the optical path. *Nat Photonics* **15**, 287–296 (2021).
18. Zhu L, Wei JX, Dong L et al. Multi-dimensional meta-holography encrypted by orbital angular momentum, frequency, and polarization. *Laser Photon Rev* **18**, 2301362 (2024).
19. Deng ZL, Jin MK, Ye X et al. Full-color complex-amplitude vectorial holograms based on multi-freedom metasurfaces. *Adv Funct Mater* **30**, 1910610 (2020).
20. Wang FL, Geng GZ, Wang XQ et al. Visible achromatic metalens design based on artificial neural network. *Adv Opt Mater* **10**, 2101842 (2022).
21. Yu ZP, Gao XY, Yao J et al. A spatial-frequency patching metasurface enabling super-capacity perfect vector vortex beams. *eLight* **4**, 21 (2024).
22. Wen DD, Cadusch JJ, Meng JJ et al. Light field on a chip: metasurface-based multicolor holograms. *Adv Photonics* **3**, 024001 (2021).
23. Yu ZJ, Li MX, Xing ZY et al. Genetic algorithm assisted meta-atom design for high-performance metasurface optics. *Opto-Electron Sci* **3**, 240016 (2024).

24. He T, Zhang JY, Tsai DP et al. A review on optical torques: from engineered light fields to objects. *Opto-Electron Sci* **4**, 250014 (2025).
25. Guo YH, Zhang SC, Pu MB et al. Spin-decoupled metasurface for simultaneous detection of spin and orbital angular momenta via momentum transformation. *Light Sci Appl* **10**, 63 (2021).
26. He HY, Lai FX, Zhang Y et al. Spectro-polarimetric detection enabled by multidimensional metasurface with quasi-bound states in the continuum. *Opto-Electron Adv* **8**, 250015 (2025).
27. Nan T, Zhao H, Guo JY et al. Generation of structured light beams with polarization variation along arbitrary spatial trajectories using tri-layer metasurfaces. *Opto-Electron Sci* **3**, 230052 (2024).
28. Yang ZJ, Huang PS, Lin YT et al. Asymmetric full-color vectorial meta-holograms empowered by pairs of exceptional points. *Nano Lett* **24**, 844–851 (2024).
29. Guo JJ, Zhang YP, Ye H et al. Spatially structured-mode multiplexing holography for high-capacity security encryption. *ACS Photonics* **10**, 757–763 (2023).
30. Qu KN, Wang ZJ, Li Z et al. Vectorial-manipulating encryption for multi-channel capacity and security enhancement. *Laser Photon Rev* **17**, 2300105 (2023).
31. Ding F, Chang BD, Wei QS et al. Versatile polarization generation and manipulation using dielectric metasurfaces. *Laser Photon Rev* **14**, 2000116 (2020).
32. Wang YZ, Pang C, Qi JR. 3D reconfigurable vectorial holography via a dual-layer hybrid metasurface device. *Laser Photon Rev* **18**, 2300832 (2024).
33. Bao YJ, Ni JC, Qiu CW. A minimalist single-layer metasurface for arbitrary and full control of vector vortex beams. *Adv Mater* **32**, 1905659 (2020).
34. Liu YF, Zhou L, Wen YZ et al. Optical vector vortex generation by spherulites with cylindrical anisotropy. *Nano Lett* **22**, 2444–2449 (2022).
35. Liu T, Dai CH, Wang DY et al. High-efficiency vectorial holography based on ultra-thin metasurfaces. *Adv Photonics* **7**, 056004 (2025).
36. Feng C, He T, Shi YZ et al. Diatomic metasurface for efficient six-channel modulation of jones matrix. *Laser Photon Rev* **17**, 2200955 (2023).
37. Zhang S, Lin PC, Huo PC et al. Broadband complex amplitude-modulated metasurfaces for nanoprinting and vectorial hologram with continuously varying linear polarization distributions. *Adv Opt Mater* **12**, 2401227 (2024).
38. Deng ZL, Deng JH, Zhuang X et al. Diatomic metasurface for vectorial holography. *Nano Lett* **18**, 2885–2892 (2018).
39. Zhang SF, Huang LL, Li X et al. Dynamic display of full-stokes vectorial holography based on metasurfaces. *ACS Photonics* **8**, 1746–1753 (2021).
40. Yu ZP, Gao XY, Yao J et al. Spin-orbit-locking vectorial metasurface holography. *Adv Mater* **37**, 2415142 (2025).
41. Zhao RZ, Sain B, Wei QS et al. Multichannel vectorial holographic display and encryption. *Light Sci Appl* **7**, 95 (2018).
42. Kim H, Jung J, Shin J. Bidirectional vectorial holography using Bi-layer metasurfaces and its application to optical encryption. *Adv Mater* **36**, 2406717 (2024).
43. Bomzon Z, Kleiner V, Hasman E. Computer-generated space-variant polarization elements with subwavelength metal stripes. *Opt Lett* **26**, 33 (2001).
44. Zeng JW, Li L, Yang XD et al. Generating and separating twisted light by gradient-rotation split-ring antenna metasurfaces. *Nano Lett* **16**, 3101–3108 (2016).
45. Bomzon Z, Biener G, Kleiner V et al. Space-variant Pancharatnam-Berry phase optical elements with computer-generated subwavelength gratings. *Opt Lett* **27**, 1141 (2002).

Acknowledgements

This work was supported by the National Natural Science Foundation of China (NSFC) (Nos. 62125503, 62375098, 62261160388), the Natural Science Foundation of Hubei Province of China (No. 2023AFA028), the Hubei Optical Fundamental Research Center (No. HBO2025TQ004), and the Technology Innovation Program of Hubei Province (Major Science and Technology Project) (No. 2024BAA001, 2024BAA005).

Author contributions

J.W. and J.W.Z. conceived the idea of the work. D.H. and Y.W. fabricated the devices. D.H. carried out the experiments. Y.D., Y.W., X.Z. and T.W. provided technical supports. D.H., J.W.Z. and J.W. performed the theoretical analyses, analyzed the data, and contributed to writing the paper. J.W. and J.W.Z. revised and finalized the paper. J.W. supervised the project.

Competing interests

The authors declare no competing financial interests.

Data availability

All data needed to evaluate the conclusions in the paper are present in the paper and supporting information. Additional data related to this paper may be requested from the authors.

Supplementary information

Supplementary information for this paper is available at https://doi.org/10.29026/oea.2026.250281

Published by Editorial Office of *Opto-Electronic Advance*, Institute of Optics and Electronics, Chinese Academy of Sciences.